



HAL
open science

Laser synthesized TiO₂ -based nanoparticles and their efficiency in the photocatalytic degradation of linear carboxylic acids

Sarah Bouhadoun, Chantal Guillard, Sébastien Sorgues, Alexandre Hérisan, Christophe Colbeau-Justin, Frederic Dapozze, Aurélie Habert, Vincent Maurel, Nathalie Herlin-Boime

► To cite this version:

Sarah Bouhadoun, Chantal Guillard, Sébastien Sorgues, Alexandre Hérisan, Christophe Colbeau-Justin, et al.. Laser synthesized TiO₂ -based nanoparticles and their efficiency in the photocatalytic degradation of linear carboxylic acids. *Science and Technology of Advanced Materials*, 2017, 18, pp.805 - 815. 10.1080/14686996.2017.1379858 . cea-01623922

HAL Id: cea-01623922

<https://cea.hal.science/cea-01623922v1>

Submitted on 25 Oct 2017

HAL is a multi-disciplinary open access archive for the deposit and dissemination of scientific research documents, whether they are published or not. The documents may come from teaching and research institutions in France or abroad, or from public or private research centers.

L'archive ouverte pluridisciplinaire **HAL**, est destinée au dépôt et à la diffusion de documents scientifiques de niveau recherche, publiés ou non, émanant des établissements d'enseignement et de recherche français ou étrangers, des laboratoires publics ou privés.



Laser synthesized TiO₂-based nanoparticles and their efficiency in the photocatalytic degradation of linear carboxylic acids

Sarah Bouhadoun, Chantal Guillard, Sébastien Sorgues, Alexandre Hérisan, Christophe Colbeau-Justin, Frederic Dapozze, Aurélie Habert, Vincent Maurel & Nathalie Herlin-Boime

To cite this article: Sarah Bouhadoun, Chantal Guillard, Sébastien Sorgues, Alexandre Hérisan, Christophe Colbeau-Justin, Frederic Dapozze, Aurélie Habert, Vincent Maurel & Nathalie Herlin-Boime (2017) Laser synthesized TiO₂-based nanoparticles and their efficiency in the photocatalytic degradation of linear carboxylic acids, Science and Technology of Advanced Materials, 18:1, 805-815, DOI: [10.1080/14686996.2017.1379858](https://doi.org/10.1080/14686996.2017.1379858)

To link to this article: <http://dx.doi.org/10.1080/14686996.2017.1379858>



© 2017 The Author(s). Published by National Institute for Materials Science in partnership with Taylor & Francis



[View supplementary material](#)



Published online: 25 Oct 2017.



[Submit your article to this journal](#)



[View related articles](#)



[View Crossmark data](#)

Laser synthesized TiO₂-based nanoparticles and their efficiency in the photocatalytic degradation of linear carboxylic acids

Sarah Bouhadoun^a, Chantal Guillard^b, Sébastien Sorgues^d, Alexandre Hérisan^d, Christophe Colbeau-Justin^d, Frederic Dapozze^b, Aurélie Habert^a, Vincent Maurel^c and Nathalie Herlin-Boime^a

^aNIMBE, CEA, CNRS, Université Paris Saclay, Gif sur Yvette, France

^bInstitut de recherche sur la catalyse et l'environnement, IRCELYON, CNRS-University of Lyon, Villeurbanne, France

^cUniv. Grenoble Alpes, CEA, CNRS, INAC, SyMMES, Grenoble, France

^dLaboratoire de chimie physique, UMR 8000-CNRS, Université Paris Saclay, Orsay, France

ABSTRACT

Titanium dioxide nanoparticles were synthesized by laser pyrolysis, their surface and electronic properties were modified by gold and/or nitrogen. These materials were characterized by different techniques like X-ray diffraction (XRD), X-ray photoelectron spectroscopy (XPS) and electron paramagnetic resonance (EPR). Time resolved conductivity (TRMC) was used to study the charge separation of electron/hole pairs. Altogether (XPS, EPR, TRMC), the physicochemical characterizations are well correlated with chemical photoactivity of the different samples. Their photocatalytic activity was evaluated for the degradation of linear carboxylic acids (C2-C3) under UV and visible illumination. The decomposition rate of acids was measured, it shows that the modification with gold increases the photoactivity while the presence of nitrogen slows down the process. Such observations are in good agreement with evolution of TRMC signals. A degradation pathway has been determined by identification of intermediate products by chromatography and EPR, results show different intermediate species. In particular EPR confirms the presence of NO²⁻ paramagnetic centers and shows two novel N centered paramagnetic centers. A decrease of the degradation rate is observed with increase of carboxylic acid chain length.

ARTICLE HISTORY

Received 22 June 2017

Revised 12 September 2017

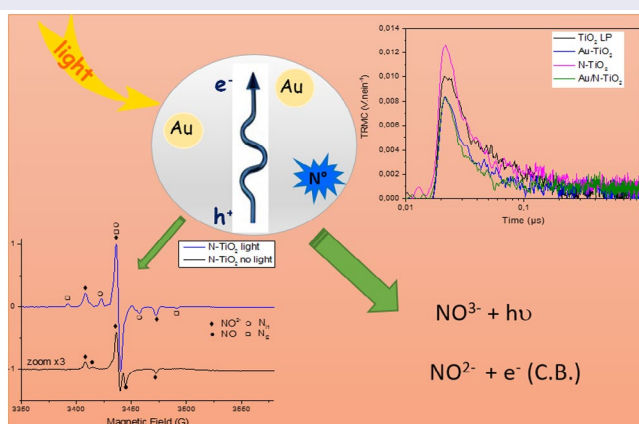
Accepted 12 September 2017

KEYWORDS

Titanium dioxide nanoparticles; gold nanoparticles; co-modification with nitrogen; time resolved microwave conductivity; photocatalysis; Electronic Paramagnetic resonance

CLASSIFICATION

60 New topics / Others; 205 Catalyst / Photocatalyst / Photosynthesis; 502 Electron spectroscopy; 305 Plasma / Laser processing, Gas phase Synthesis; 600 Time Resolved Microwave Conductivity




1. Introduction

Many studies deal with the fabrication and characterization of the photocatalytic activity of various materials exhibiting efficiency both in the visible and UV range [1–3]. In particular, materials based on TiO₂ are intensively studied due to their high activity under UV illumination. The main drawbacks are high recombination rate and lack of activity under visible light. Improving photocatalytic efficiency under visible illumination would

allow taking advantage of solar irradiation that is a free, abundant and non-polluting energy [4–7]. Different ways to enhance the visible photoactivity are doping by hetero-elements (N, S, F, ...) or introducing metallic structures (Au, Ag, ...) with an absorption in the visible range and/or able to improve the charge separation [8–14]. In this context, we have previously demonstrated that the laser pyrolysis is an efficient method for the one step synthesis of TiO₂-based nanomaterials (Au/TiO₂,

CONTACT Nathalie Herlin-Boime  nathalie.herlin@cea.fr

 The supplemental material for this paper is available online at <https://doi.org/10.1080/14686996.2017.1379858>

© 2017 CEA, Commissariat à l'Énergie Atomique et aux Énergies Alternatives. Published by National Institute for Materials Science in partnership with Taylor & Francis.

This is an Open Access article distributed under the terms of the Creative Commons Attribution License (<http://creativecommons.org/licenses/by/4.0/>), which permits unrestricted use, distribution, and reproduction in any medium, provided the original work is properly cited.

N-TiO₂ and co-modified Au/N-TiO₂) [15]. Under UV illumination, these samples were very efficient for the degradation of formic acid by comparison with commercial TiO₂ P25. In particular gold modification of titanium dioxide enhances transfer of electrons. Interestingly, a significant activity was observed under visible illumination for our both materials containing nitrogen [15].

In parallel to materials development, advanced characterization methods are used to study their characteristics (crystallization in preferred directions, surface states,...) and correlate them to photocatalytic properties [14,16,17]. Previous EPR studies have shown the existence of paramagnetic nitrogen species interacting with the TiO₂ lattice. These paramagnetic species are involved in the photo-induced electron transfer from the solid to an electron scavenger such as molecular oxygen [3,17,18]. Time Resolved Microwave Conductivity (TRMC) was used to demonstrate that Au nanoparticles can act as electron scavengers retarding recombination in Au-TiO₂ samples [14,19]. In this paper, we apply TRMC to characterize the ability of our sample to study charge carrier dynamics under UV or visible illumination. Based on TRMC and EPR results giving information on the presence of paramagnetic centers, we establish a qualitative classification in our family of samples towards their ability to separate the charges. Indeed, it is well known that charge separation is of major importance in the efficiency of photocatalyst materials [20]. In combination with other methods (such as X-ray photoelectron spectroscopy (XPS), EPR and photoluminescence [15]), we use the information obtained from TRMC to correlate the physicochemical properties to photocatalytic activity, i.e. ability of these samples to decompose various linear (C1 – C3) acids under UV or visible light. Indeed, by using different excitation wavelengths, TRMC gives information on the number of exciton created under UV or visible illumination for one type of sample and therefore predict their relative photocatalytic efficiency under both types of illumination.

2. Experimental details

2.1. Chemicals

Titanium tetraisopropoxide (TTIP, 97% purity) and hydrogen tetrachloroaurate (III) HAuCl₄•3H₂O were respectively used as titanium source for synthesis of TiO₂ nanoparticles, as gold source. Ammoniac (NH₃) gas was supplied by Messer. These reactants and the carboxylic acids CH₃COOH, and CH₃CH₂COOH were obtained from Sigma-Aldrich and used without further purification. Commercial reference TiO₂ P25 was obtained from Evonik.

2.2. Synthesis

Modified nanoparticles (NPs) were synthesized through laser pyrolysis method by using HAuCl₄•3H₂O dissolved

in TTIP and NH₃ as precursors. Briefly, this method is based on the interaction between a flow of precursors and a high power CO₂ laser beam. The reactants are heated and dissociated with appearance of a flame. Homogeneous nucleation occurs; nanoparticles grow in the hot zone and are collected downstream on metallic filters. More details were reported in our previous work [15].

The obtained powders were annealed at 400 °C under air flow (650 cm³ min⁻¹) in an oven (Pyrox) during 3 h to remove the residual carbon due to the decomposition of reactants (TTIP). All the results presented here concern annealed powders.

2.3. Characterization methods

The identification of crystallite phase of the synthesized photocatalysts was carried out by X-ray Diffraction measurements (XRD, Siemens D5000 diffractometer with Cu-K α radiation ($\lambda = 1.54184 \text{ \AA}$)). The 2θ angle ranged from 20° to 80° with a step size of 0.04° and a counting time of 7s/step. The average TiO₂ crystallite size of the sample was calculated from the Scherrer equation. The chemical environment of nitrogen atoms in TiO₂ was deduced by X-ray photoelectron spectra (XPS) (Kratos Analytical Axis Ultra DLD spectrometer, Al K α X-ray) on the powders.

The charge-carrier lifetimes in TiO₂ after UV and visible illumination were determined by TRMC [21,22]. The TRMC technique is based on the measurement of the change of the microwave power reflected by a sample, $\Delta P(t)$, induced by its laser pulsed illumination. The relative difference $\Delta P(t)/P$ can be correlated, for small perturbations of conductivity, to the difference of the conductivity $\Delta\sigma(t)$ considering the following equation:

$$\frac{\Delta P(t)}{P} = A\Delta\sigma(t) = Ae \sum_i \Delta n_i(t)\mu_i$$

where $\Delta n_i(t)$ is the number of excess charge-carriers i at time t and μ_i their mobility. The sensitivity factor A is independent of time, but depends on different factors such as the microwave frequency or the dielectric constant. Considering that the trapped species have a small mobility, which can be neglected, Δn_i is reduced to mobile electrons in the conduction band and holes in the valence band. And in the specific case of TiO₂, the TRMC signal can be attributed to electrons because their mobility is much larger than that of the holes [23].

The incident microwaves were generated by a Gunn diode of the K α band at 30 GHz. Pulsed light source was an optical parametric oscillator (OPO, EKSPLA, NT342B) tunable from 225 to 2000 nm. It delivers 8 ns pulses (full width at half maximum) with a frequency of 10 Hz. The light energy densities received by the sample were respectively 1.2, 3.4, and 7.0 mJ•cm⁻² at 355, 410, and 450 nm. The main data provided by TRMC are given by the maximum value of the signal (I_{max}), which reflects

the number of the excess charge-carriers created by the pulse and the decay of the signal $I(t)$, which is due to the decrease of the excess electrons controlled by recombination and trapping.

Low-temperature continuous-wave EPR spectra were recorded with a Bruker EMX spectrometer operating at X-band (9.65 GHz) frequency and equipped with an ER-4116 dual mode cavity and an Oxford Instruments ESR-900 flow cryostat. For the study of photoirradiated dry photocatalyst powders, *in situ* irradiation of samples in the EPR cavity was achieved using a fibered Schott KL1500 halogen UV-visible lamp. For the study of degradation of carboxylic acids (0.1 M) in aqueous dispersion of photocatalyst (4 g L⁻¹), the samples were frozen in liquid nitrogen and irradiated in a Rayonet UVA photoreactor (8 mW cm⁻²) for 30 min at T = 77 K in a quartz cold finger, then transferred into the EPR spectrometer at T = 60 K.

2.4. Photocatalytic experiments

The photocatalytic efficiency of samples was evaluated by following the degradation of linear acids (1086 μmol L⁻¹) in water and 181 μmol L⁻¹ corresponding to a similar concentration of carbon. The photocatalytic tests were carried out in a Pyrex photoreactor. For UV irradiation, a mercury lamp Phillips HPK 125 W with optical filters 7.6 and 0.52 (Corning) were employed to obtain an emission peak centered at $\lambda = 365$ nm. The radiant flux at 4.2 mW cm⁻² (7.7 10¹⁵ photons s⁻¹ cm⁻²) was measured using a VLX-3 W radiometer with 365 nm sensor. For visible light illumination in the region (400–800 nm), LED lamp was used; the photon flux was measured around 85 10⁻³ μmol s⁻¹. Both lamps were placed at the bottom of the reactor; the illuminated area was 12.5 cm². Circulating water between lamp and reactor maintain the solution temperature at 20 °C. Before irradiation, the system with TiO₂ concentration of 1 g L⁻¹ was always stirred in the dark for 30 min, to reach the adsorption-desorption equilibrium of carboxylic acids on surfaces.

At regular time intervals of irradiation, aliquots of each acid suspension was collected, filtered using 0.45 μm Millipore filters before analysis. The concentrations of acids remaining after adsorption and during the photocatalytic degradation process were determined by high-performance liquid chromatography (HPLC) analysis. VARIAN Prostar HPLC apparatus equipped with a single-wavelength UV-vis detector and a 300 mm x 7.8 mm carbohydrate analysis column (COREGEL-87H3) was used. The mobile phase was H₂SO₄ solution (5 10⁻³ mol L⁻¹) and the flow rate was fixed at 0.7 cm³ min⁻¹. The detection wavelength was set at 210 nm.

3. Results and discussion

Based on our previous synthesis and photocatalytic results [15], four samples were selected for this study. The samples are TiO₂ LP, Au/TiO₂, N-TiO₂ and

co-modified Au/N-TiO₂ and their main characteristics are presented in Table S1. The samples were synthesized by laser pyrolysis in similar conditions, except the choice of the reactive mixture injected in the laser beam. The TiO₂ LP was chosen as a reference and for comparison with TiO₂ P25, Au/TiO₂ sample was selected to demonstrate the effect of the metallic additive. N-TiO₂ was chosen because its visible activity is well known [24,25]. In addition the co-modified Au/N-TiO₂ sample exhibiting significant activity in the visible while maintaining good activity under UV illumination is part of the study [26,27].

3.1. XRD and XPS characterization of materials

XRD patterns of pure and modified TiO₂ powders [15] show a major anatase crystallite phase with less than 5% of rutile (Figure S1), this ratio was estimated from the peaks located at $2\theta = 25.32^\circ$ (anatase) and at $2\theta = 27.45^\circ$ (rutile). The anatase crystallite size was evaluated using the Scherrer equation. The mean crystallite size deduced from XRD measurements is in the range 7–9 nm for all these samples, in quite good agreement with the grain size deduced from transmission electron microscopy measurements (Table S1).

The XPS spectra of all nitrogen-doped and gold modified TiO₂ have been recorded. The spectra corresponding to Ti 2p and O 1s levels are shown in Figure S2. As usually observed for the Ti 2p spectra, two peaks are present at 458.5 eV and 464.3 eV assigned to Ti 2p_{3/2} and Ti 2p_{1/2} in agreement with the presence of Ti⁴⁺ in a TiO₂ environment. The O 1s binding energies of all powders were located at energies slightly higher than 530 eV, attributed to O²⁻ in the TiO₂ lattice. Let us note the Au could not be detected, probably due to the low content below the detectivity level of XPS. In the N-doped samples (N-TiO₂ and Au/N-TiO₂), the N local environment has also been studied. The spectra and fitting curves are presented in Figure 1 (The spectrum of Au/N-TiO₂ sample is very similar and is therefore not shown here). Two peaks are present; their binding energies at 399.7 and 401.7 eV as already observed in the literature and are assigned to O-Ti-N bonds (interstitial N) [18,28,29] and to molecularly adsorbed N species like NO or NO₂ molecules on the particle surface [30], respectively. It is therefore important to note here that a significant part of our nitrogen is located at the surface of nanoparticles.

3.2. EPR study of charge carriers and paramagnetic species

N-doped and Au-modified samples (Au/TiO₂, N-TiO₂ and Au/N-TiO₂) were also studied by EPR at low temperature (60 K) in the dark as well as in the presence of UV-visible light irradiation (Figure 2).

Looking at the EPR spectrum recorded for Au/TiO₂ samples, (Figure 2(a)), the signal in the dark is of weak

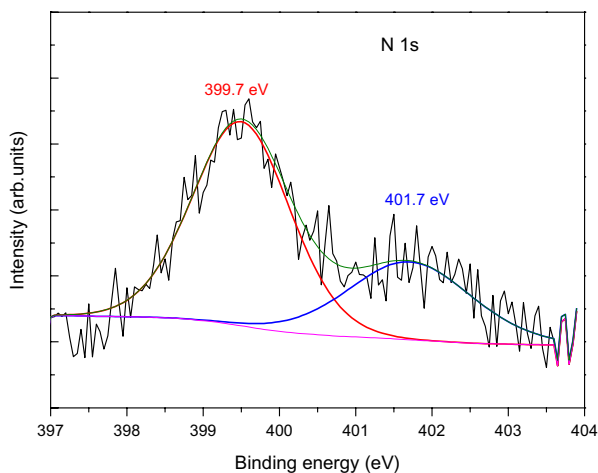


Figure 1. XPS spectrum of N-TiO₂ powder.

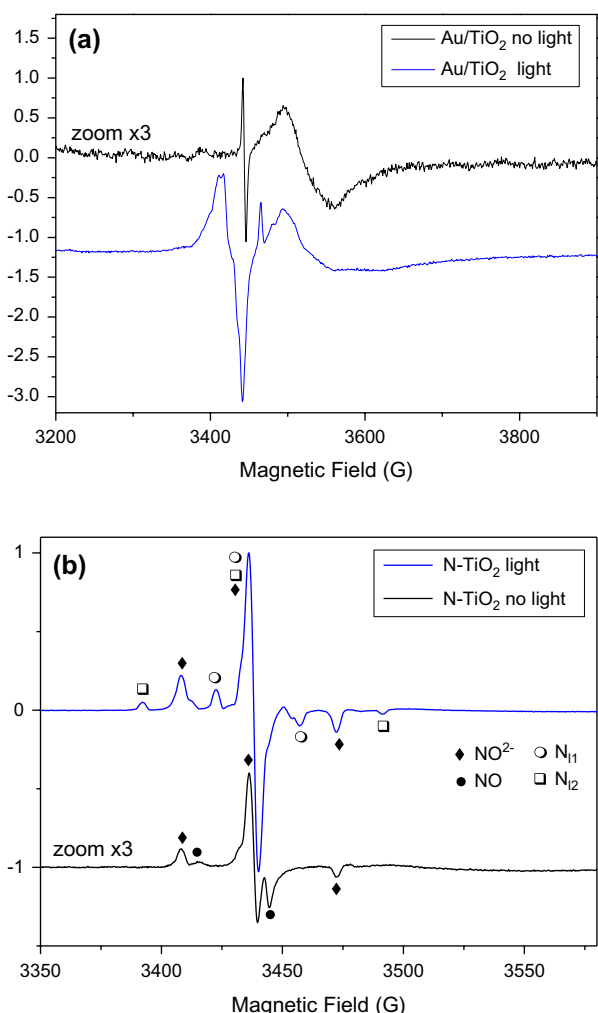


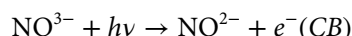
Figure 2. EPR spectra observed for dry photocatalysts powder without (dark curves) and with (blue curves) *in situ* UV-visible (halogen-lamp) irradiation at T = 60 K. (see exp. section for details). (a) Au modified sample, (b) N-doped sample.

intensity. It is composed of a broad part due to trapped electrons (Ti³⁺ in rutile and surface Ti³⁺, Table 1) and a sharp line at g = 2.002 tentatively attributed to bulk

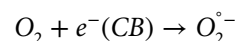
anion vacancy defects [31]. Such signals were previously reported in EPR studies of Au/TiO₂ catalysts prepared by deposition/precipitation methods [31]. Under UV-visible light irradiation, this sample exhibits much more intense EPR signals due mostly to the presence of charge carriers. Trapped electrons including Ti³⁺ in rutile, Ti³⁺ in anatase and Ti³⁺ in surface sites are observed at g values lower than 2. Holes trapped in anatase and or rutile phases are also observed with signals at g = 2.021 and 2.018 (Table 1 and [32]). The remaining smaller features at g > 2 can be attributed to O₂⁻ stabilized at anatase surface or Ti⁴⁺O²⁻Ti⁴⁺O⁻ sites [31,32].

The EPR spectrum recorded for N-TiO₂ (Figure 2(b)) in the dark is much more intense than the spectrum of Au/TiO₂ in the dark, as also shown by the signal to noise ratio, and different species are present. By numerical simulation of the EPR spectrum (Figure S3), it was possible to identify four main species with important contributions in the EPR spectrum : surface Ti³⁺ with similar g tensor as reported for C-doped TiO₂ [33], a second surface Ti³⁺ site similar to the one observed for Au/TiO₂, NO^o radicals [34,35] and a last paramagnetic center exhibiting nitrogen hyperfine splitting. This signal was attributed to a nitrogen center labeled as N_b^o in many papers in the literature [18,35,36], then attributed to interstitial or substitutional N atom in TiO₂ [16] and finally identified as paramagnetic NO²⁻ species trapped in bulk TiO₂ [17,37]. When the sample is irradiated *in situ* with halogen lamp, the spectrum changes drastically (Figure 2(b)). The contributions of Ti³⁺ in rutile, surface Ti³⁺ and NO^o radical vanish. Signal from holes is no more observed. The signal due to NO²⁻ increases by a factor of five and two new paramagnetic centers exhibiting different N hyperfine coupling appear (named N₁₁^o and N₁₂^o in Table 1).

The increase of EPR signal attributed to NO²⁻ centers in N-TiO₂ samples under visible or UV-visible irradiation has been already observed [37,38] and was rationalized by Barolo et al. [37]. These authors report the presence in the synthesized nanoparticles of a diamagnetic center (NO³⁻). This species is responsible of the visible absorption in N-TiO₂ materials. It does not create [electron-hole] pairs in N-TiO₂, but rather promote an electron from diamagnetic NO³⁻ intraband gap states to the conduction band, thus creating more paramagnetic NO²⁻ intraband gap states.



The produced electron is transferred onto the scavenger (O₂) to form O₂²⁻



On the other hand to the best of our knowledge the two other paramagnetic centers exhibiting different N hyperfine coupling have not been described in the literature.

Table 1. EPR parameters of species observed for dry photocatalysts powders.

	g tensor			A _N tensor (G)			Reference
	(g ₁ ≥ g ₂ ≥ g ₃)			(A ₁ , A ₂ , A ₃) in g frame			
Bulk anion vacancy	2.002			–			Okumura et al. [31]
Ti ³⁺ anatase	1.990	1.990	1.960	–			Kumar et al. [32]
Ti ³⁺ rutile	1.970	1.970	1.944	–			Kumar et al. [32]
Surface Ti ³⁺ at pH 10	1.945	1.945	1.885	–			Howe and Grätzel [39]
rutile TiO ₂ (Ti ⁴⁺ O ²⁻ -Ti ⁴⁺ OH ⁻)	2.019	2.014	2.002	–			Kumar et al. [32]
anatase TiO ₂ (Ti ⁴⁺ O ²⁻ -Ti ⁴⁺ OH ⁻)	2.016	2.012	2.002	–			Kumar et al. [32]
Ti ³⁺ surface reported for C-doped	1.971	1.971	1.948	–			Li et al. [33]
NO ^o	2.001	1.998	1.927	<1	32.2	9.6	Livraghi et al. [34][35]
NO ²⁻	2.005	2.004	2.003	2.3	4.4	32.2	Livraghi et al. [17]
N ₁₁ ^o	2.007	2.055	2.003	–	–	17.2	This work
N ₁₂ ^o	2.005	2.004	2.0023	–	–	49.5	This work

They disappear when the sample is warmed up to room temperature and were observed only during or just after irradiation at low temperature, so they will be named N₁₁^o and N₁₂^o hereafter (the subscript ‘l’ stands for ‘light’).

The EPR spectrum recorded for Au/N-TiO₂ (Figure S4) in the dark exhibits only NO²⁻ paramagnetic centers. No contribution from NO neither from Ti³⁺ was observed. Under UV-visible irradiation the EPR spectrum is comparable to this observed for N-TiO₂ but approximately twice less intense: the same paramagnetic centers NO²⁻, N₁₁^o and N₁₂^o are observed under UV-vis irradiation.

Finally, by comparing the EPR spectra recorded with UV-visible irradiation of Au/TiO₂, N-TiO₂ and Au/N-TiO₂ in exactly the same conditions, one can see that nitrogen doping induces drastic changes. UV-visible photoirradiated Au/TiO₂ exhibits both EPR signals due to holes and electrons as observed in classical TiO₂ samples. On the opposite, no EPR signal from holes nor photogenerated electrons could be observed in N-TiO₂ and Au/N-TiO₂. So according to these results N containing samples produce much less electron and holes than Au/TiO₂ under UV-visible irradiation. Instead of producing holes, photoirradiation promotes mainly the formation of paramagnetic NO²⁻ species which may induce a less good reactivity for the photooxidation of carboxylic acids.

3.3. Charge carrier dynamics

The electronic properties of the samples were studied by TRMC technique considering both UV and visible regions. The excitation wavelengths were 355 and 450 nm. Let us note that such comparison of the samples is possible because all the samples were obtained by the same method in similar conditions

3.3.1. UV excitation (355 nm)

Figure 3 presents the TRMC signals recorded for the different samples after UV excitation. In Table 2, column 2 gives the maximum value of the signal proportional to the number of excitons created under illumination while column 3 allows comparison of the short range

decay behavior of the different samples. Column 4 presents the K_D adimensional parameter related to long-term lifetime of charge carriers (after 100 ns), higher K_D corresponds to faster decays of the TRMC signal. This parameter is obtained using the $I = I_D \times t^{-k_D}$ expression as proposed in the paper of Meichtry et al. [40]. Figure 3 shows similar behavior for all the samples : a classical anatase signal achieving a maximum value at about 20–25 ns followed by an anatase long decay with recombination phenomena at short-time range (0 to 40 ns) and trapping phenomena at longer-time range (after 40 ns) and mainly noise after 100 ns [41,42]. The 0.18 and 0.19 k_D values obtained for samples containing gold show that there is almost no slow processes (after 100 ns) in these samples. Considering the TiO₂ LP and N-TiO₂ samples, the higher k_D values indicate the presence of phenomena occurring at long-time range such as decay of excess electrons [40] in good agreement with the higher number of electrons in these samples (Figure 3). The influence of the incorporated gold can be also observed by comparing the signals measured on TiO₂ and Au/TiO₂ materials (Figure 3). First, at short-time range, gold acts like an impurity. It can be observed by the reduction of I_{max} and a lower value of I_{40 ns}/I_{max} (0.34 compared to 0.27 in Table 2), corresponding to a faster decay of the electrons population in Au/TiO₂ sample. This decay can be associated either to recombination phenomena or transfer of charges. In this case, photoluminescence experiments have already indicated an electronic transfer from TiO₂ to gold, therefore the TRMC result can be safely attributed to the transfer of electrons to gold and is in good agreement with an improved photocatalytic activity of Au/TiO₂ in comparison with TiO₂ LP as already observed for the degradation of formic acid (FA). Indeed, the effect of Au and/or Cu metallic additives on P25 was studied by TRMC [19]. It induced a faster transfer of electrons to the surface correlated to an improved photocatalytic efficiency similar to our present work.

If we now turn to the N-doped sample, a first effect can be seen at short-time range. I_{max} is slightly higher for the N-doped compound (84 mV vs 69 mV for the TiO₂ sample) indicating a better charge-carrier creation.

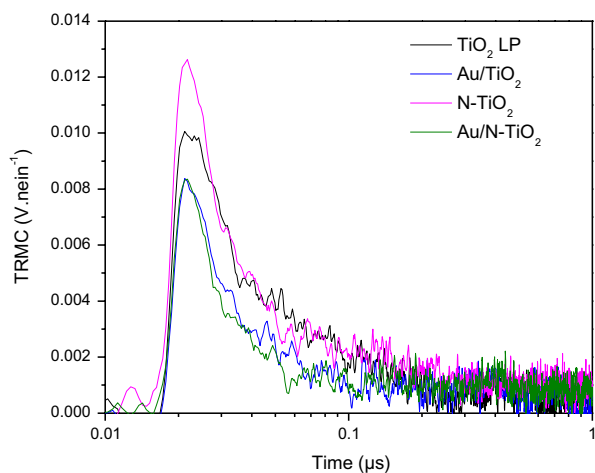


Figure 3. TRMC signal of pure and modified TiO_2 obtained by irradiation at 355 nm.

Table 2. TRMC parameters for pure and modified TiO_2 obtained by irradiation at 355 nm.

Sample	I_{max} ($\text{V}\cdot\text{nein}^{-1}$)*	I_{max} (mV)	$I_{40\text{ ns}}/I_{\text{max}}$	k_{D}
TiO_2 LP	0.010	69	0.34	0.67
Au/TiO_2	0.008	55	0.27	0.19
N-TiO_2	0.013	84	0.22	0.36
$\text{Au}/\text{N-TiO}_2$	0.08	55	0.16	0.18

* $\text{V}\cdot\text{nein}^{-1}$ stands for Volt per nano-Einstein, i.e. mol of photons.

However, like previously, this effect is accompanied by a faster loss of electrons (lower $I_{40\text{ ns}}/I_{\text{max}}$, 0.22 compare to 0.34) and no long-time range effects are detected: TRMC signals of pure and doped compounds are equal after 40 ns. In the N-TiO_2 samples the faster loss of electrons can be related to the presence of nitrogen in surface states as shown by XPS (Figure 1). Indeed, such surface states are known to act as recombination centers where the electrons are lost. Therefore, the N doping induces recombination which is in good agreement with the less efficient photocatalytic activity (FA degradation) observed for this sample under UV illumination [15].

The compound modified with Au and N shows the lowest $I_{40\text{ ns}}/I_{\text{max}}$ value, i.e. the fastest electron loss (0.16 vs 0.34 for TiO_2). Indeed, in this sample, both N and Au tend to decrease the electron population both by transfer to gold and charge recombination at the surface, explaining this observation. However, it is not possible to quantify the respective contribution of these effects and explain the efficiency of $\text{Au}/\text{N-TiO}_2$ by comparison to TiO_2 .

Finally, these results tend to indicate that the most active sample is Au/TiO_2 , the less active N-TiO_2 while TiO_2 and $\text{Au}/\text{N-TiO}_2$ are in between but their respective efficiency cannot be anticipated. Taking into account the very low Au amount in the powder in $\text{Au}/\text{N-TiO}_2$, it could be expected that the negative recombination effects due to N at the surface will be dominant, and explaining the lower photoactivity (degradation of FA) of $\text{Au}/\text{N-TiO}_2$ compared to TiO_2 [15].

3.3.2. Visible excitation (450 nm)

Using the photons delivered by solar light in the visible range to increase the efficiency of photocatalytic processes remains a challenge, and N doping is known to induce some photocatalytic activity in the visible range [3,43]. In a previous study, we have shown that both N-TiO_2 and $\text{Au}/\text{N-TiO}_2$ samples are efficient for the degradation of FA under visible illumination. In the same way than previously, but using visible excitation, the creation and decay of exciton was measured by TRMC for our two N-doped samples exhibit some activity under visible range [15], Figure 4 shows the TRMC signals of N-doped and Au/N co-modified TiO_2 .

The main point of these data is the very low number of excitons created after visible excitation compared to UV excitation (0.001 vs 0.01 $\text{V}\cdot\text{nein}^{-1}$). The low number of excitons is easily correlated to the existing but weak efficiency observed for degradation of FA.

However, it clearly illustrates that the efficiency of our materials under visible excitation cannot be considered significant and this point will not be studied any more in the present paper. Moreover in good agreement with this low efficiency, monochromatic visible irradiation is known in literature to produce electron and not holes [37].

3.4. Comparison of EPR and TRMC under UV irradiation

UV-visible photoirradiated Au/TiO_2 exhibits both EPR signals due to holes and electrons as observed in classical TiO_2 samples. In agreement with a high number of electrons created under UV irradiation, the TRMC signal is of high intensity. Therefore, both techniques tend to indicate efficient surface activity.

The EPR signal observed with N-modified sample is mainly attributed to paramagnetic NO^{2-} species. In TRMC, although the charge carrier creation is the highest in N-TiO_2 sample, the electrons are rapidly lost by recombination with surface traps. In fact, the NO^{2-} species seen by EPR under UV-visible irradiation (Figure 2), can act as traps for the electrons explaining the low efficiency of these samples.

3.5. Photocatalytic results

We have seen that, all our samples are significantly more active than TiO_2 P25 when degradation of FA is considered [15]. In view of addressing more realistic pollutants, our interest was to understand if this result could be extended to more complex reactants while remaining in the same family (i.e. carboxylic acids). Therefore, the degradation of carboxylic acids with more carbon atoms (up to 3) was studied.

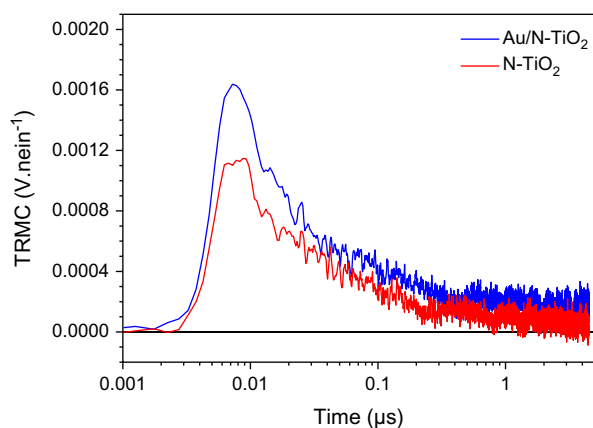


Figure 4. TRMC signal of N-TiO₂ and Au/N-TiO₂ obtained by irradiation at 450 nm.

Table 3. Adsorbed quantities of carboxylic acids at equilibrium under dark for the different reactants and catalysts ($\mu\text{mol g}^{-1}$).

Catalyst	TiO ₂ P25	TiO ₂ LP	Au/TiO ₂	N-TiO ₂	Au/N-TiO ₂
Formic acid	87	257	158	168	176
Acetic acid	60	35	70	35	35
Propionic acid	116	66	53	75	135

3.5.1. Adsorption studies

Reaction at the surface of nanoparticles is a key mechanism in photocatalysis, it is therefore fundamental to investigate the evolution of the adsorption in the dark of the different reactants on the different materials. The adsorption results are presented in Table 3. It shows that for Laser synthesized powders, adsorption is significantly higher for FA compared to other acids. The difference is not so large for the TiO₂ P25 reference sample. Table 4 shows pK_a and pH of each acid (pH was measured in solution without nanoparticles). Based on these data the ratio of ionized [A⁻] to neutral [AH] species is much higher for FA than for acetic or propionic acid. It can explain the very different adsorption of FA compared to acetic and propionic acids (257 $\mu\text{mol g}^{-1}$ compared 35 or 66 $\mu\text{mol g}^{-1}$ for example in TiO₂ LP). These results are also in agreement with the study by Serpone et al. [44] relating the adsorption behavior on TiO₂ to the degree of ionization of acids. Indeed, the lower the pK_a, the highest is the degree of ionization thereby favoring adsorption. Serpone et al. also predict a decrease of activity with the increment of the length of the carbon chain.

3.5.2. Photocatalytic degradation

Figure 5 presents the evolution of the concentration of C2 and C3 acids under UV irradiation in presence of modified TiO₂ samples. In both cases, similar tendencies can be observed; the curves show that according to their behavior, the powders can be divided into two groups. The first group is composed of N-doped TiO₂ samples; they are less active than TiO₂ LP. TRMC, XPS and EPR results have shown the presence of

Table 4. pK_a and pH of carboxylic acids (C1, C2, and C3).

Carboxylic acid	Formic acid	Acetic acid	Propionic acid
pK _a	3.75	4.75	4.87
pH	3.3	3.7	3.8
A ⁻ /AH	0.39	0.090	0.085

nitrogen species that could act as recombination center. Therefore, the lower photocatalytic result is in good agreement with behavior expected from characterization. The second group is composed of P25, TiO₂ LP and Au/TiO₂ powders presenting a similar photoactivity. As in our previous study, the modification with Au has a positive effect on the photocatalytic efficiency: (Au/N-TiO₂ and Au/TiO₂ are more active than N-TiO₂ and TiO₂ LP) [15]. Finally, the photocatalytic activity follows the order: Au/TiO₂ > TiO₂ LP \approx P25 > Au/N-TiO₂ > N-TiO₂ (Figure 6).

In comparison with our previous results on the degradation of formic acid under UV [15], kinetic decomposition of acetic acid (AA) and propionic acid (PA) is slower as illustrated in Figure 6. The kinetics of degradation of AA and PA are quite comparable, this seems correlated to adsorption very similar for most samples when these reactants are considered. In the same way, adsorption is significantly smaller for these two reactants compared to FA and the kinetics of degradation are slower, illustrating again the importance of surface reaction in the photocatalytic process. Moreover, the disappearance rates of FA, AA and PA molecules are correlated to the rate constants of OH[•] attack radicals which are 1.4 10⁸, 1.six 10⁷ and five.7 10⁶ L.mol⁻¹.s⁻¹, respectively [45].

3.6. Intermediate species and mechanism

One interest of using longer carbon chain corresponding to smaller degradation rates is the possibility to observe intermediate species giving information on the mechanisms involved in the degradation processes. Considering both formic and acetic acids, no peak could be observed in the chromatograms (HPLC) at the end of the degradation process. Therefore, EPR analyses were carried out to obtain further insight into the nature of intermediates species and to characterize the local environment of the paramagnetic species.

Figure 7 shows the EPR spectra obtained with Au/TiO₂ and N-TiO₂ samples in the presence of acetic acid, recorded at 60 K and previously irradiated in a quartz cold finger at 365 nm and 77 K. Two intermediates were well identified, they can be assigned to methyl radical $\cdot\text{CH}_3$ with a proton hyperfine interaction ($a_{\text{H,CH}_3} = 22.9\text{G}$), and to carboxymethyl radical $\cdot\text{CH}_2\text{-COOH}$ ($a_{\text{H,CH}_2} = 21.1\text{G}$). Four other narrow EPR lines (green labels in Figure 7) were observed and could be rationalized by a free radical containing two non-equivalent protons ($a_{\text{H1}} = 23.2\text{G}$, $a_{\text{H2}} = 11.4\text{G}$). To the best of our knowledge this last species was not reported to

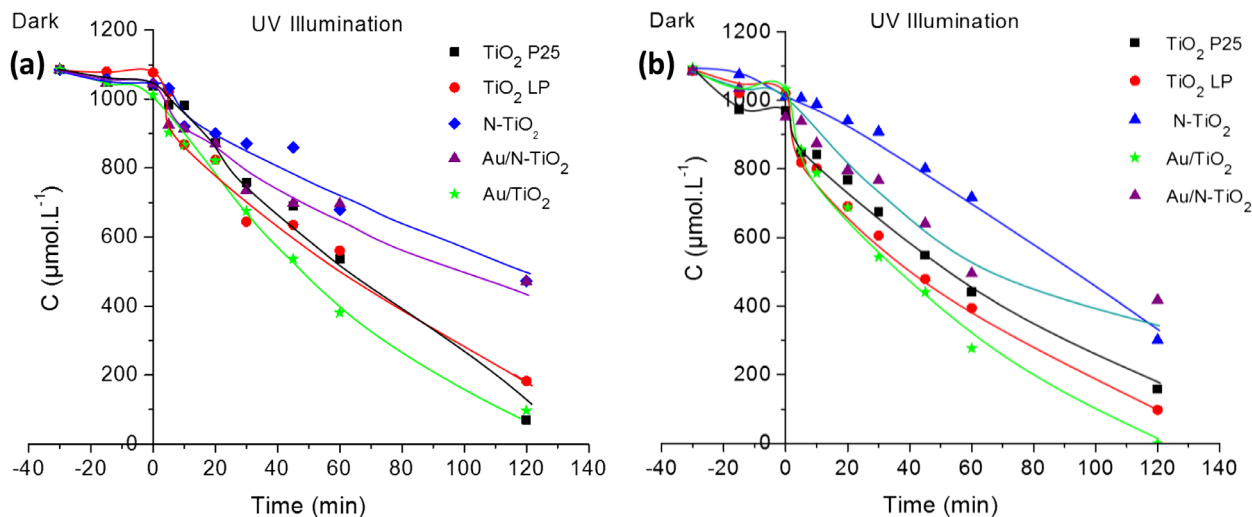


Figure 5. Photocatalytic decomposition of acetic acid (a) and propionic acid (b) under UV illumination for pure and modified TiO₂ samples (the lines are only guides for the eyes).

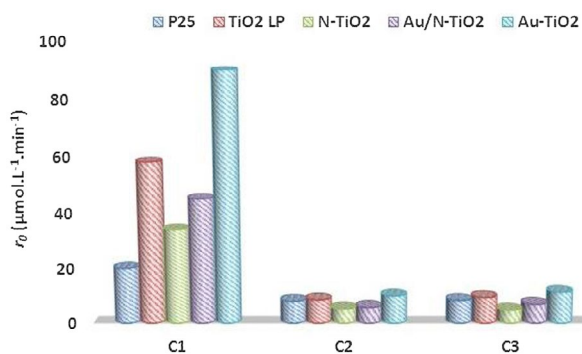
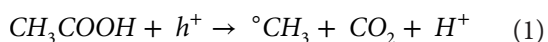


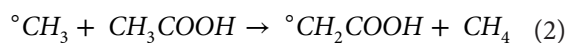
Figure 6. Evolution of the initial degradation rate (r_0) as function of carbon chain.

date in the literature of carboxylic acid photooxidation by TiO₂, and no satisfying hypothesis could be found yet to rationalize it.

The observation of methyl and carboxymethyl radicals is consistent with the results reported by Kaise et al. [46] who explain their formation by the attack of photogenerated hole of TiO₂ and then enter in the steps of photo-Kolbe reaction (Equation (1)). The same radicals were found by Nosaka et al. [47]. The formation of methyl radical is easily explained by the reaction of AA with a hole at the surface of the particle following reaction (1).



The resulting methyl radical can in turn react with AA to form carboxymethyl radical



Another possible reaction can generate the carboxymethyl radical (Equation(3)) [48]

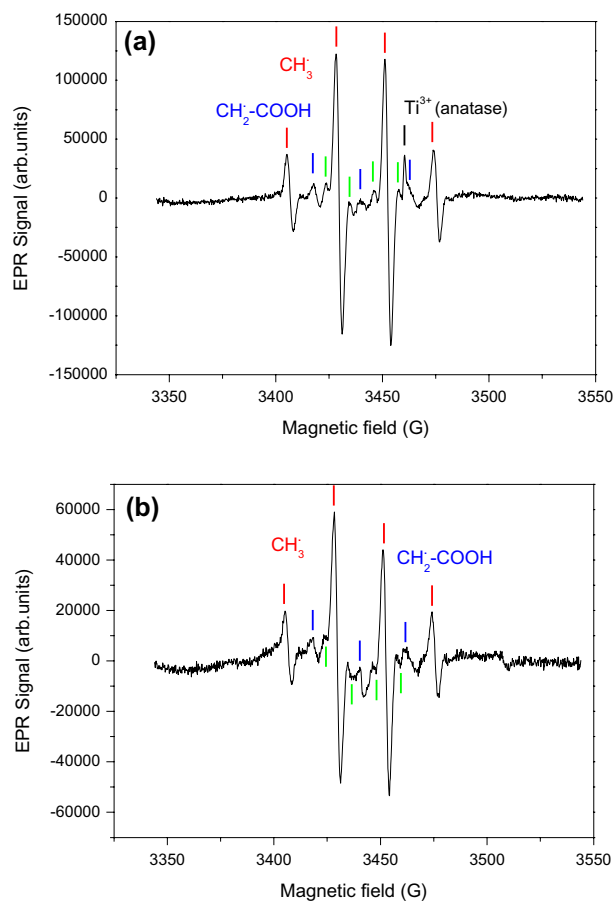
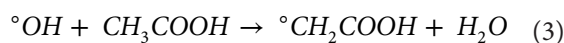


Figure 7. EPR spectra of (a) Au/TiO₂ and (b) N-TiO₂ in presence of acetic acid recorded at 77 K, and irradiated at $\lambda = 365$ nm.



These radicals can follow reaction path with O₂ to product alcohol, then aldehyde and finally CO₂ in the case of

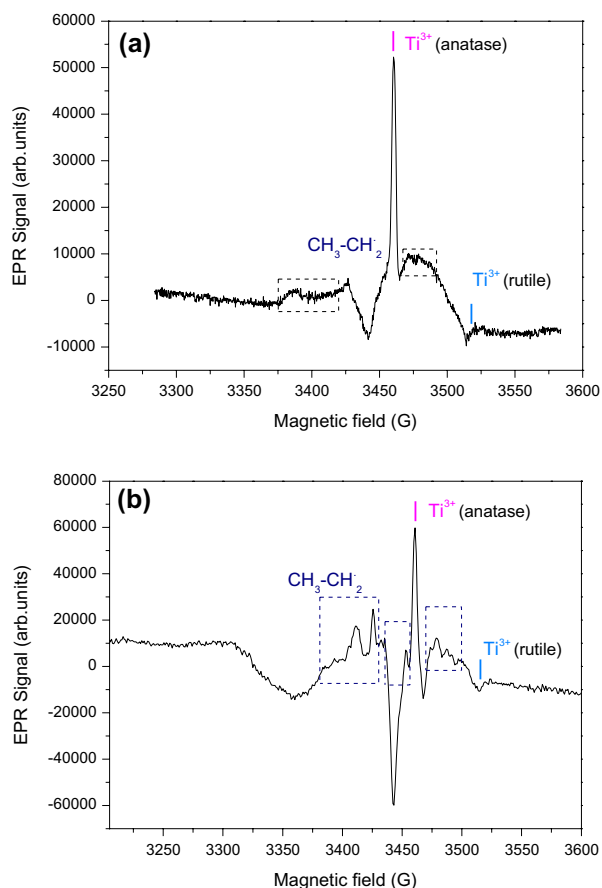
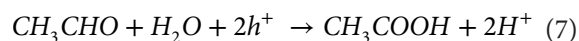
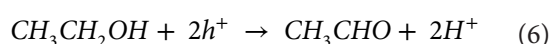
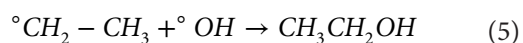
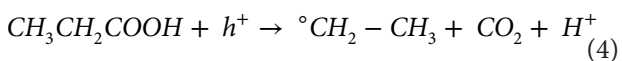


Figure 8. EPR spectra of (a) Au/TiO₂ and (b) N-TiO₂ in presence of propionic acid recorded at 77 K, and irradiated at $\lambda = 365$ nm.

$^{\circ}\text{CH}_3$ or glycolic acid, glyoxylic acid, formaldehyde and then CO₂ in the case of $^{\circ}\text{CH}_2\text{COOH}$ [48].

During propionic acid photodegradation, only acetic acid was detected by HPLC. In this case, again EPR was used to detect eventual intermediates. Figure 8 shows the EPR spectra of Au/TiO₂ and N-TiO₂ samples in presence of propionic acid, recorded at 77 K and irradiated at 365 nm. Both of spectra show the typical signals corresponding to electron (Ti³⁺ species) in anatase and rutile environment [32]. Let us note that in this case the narrow Ti³⁺ signal is easily seen by contrast to the broader features observed in the spectrum. Some of these features could be attributed to $^{\circ}\text{CH}_2 - \text{CH}_3$ radicals by comparison with observation by Shkrob and Chemerisov [49] and appeared more clearly in the experiment performed with N-TiO₂. Similarly to the observation by Shkrob and Chemerisov, the hyperfine splitting of $^{\circ}\text{CH}_2 - \text{CH}_3$ free radicals are not well resolved due to their anisotropy. Sakata et al. [50] proposed reaction path that explain the photocatalytic degradation of propionic acid (Equations (4-7)).



After these cascade reactions, the final product (acetic acid) will undergo the same reaction which was seen previously.

Finally, when HPLC could not give information (acetic acid), EPR study provides us the detection of intermediate species in the degradation mechanism in good agreement with the literature [47,49]. Considering propionic acid, EPR radicals support the presence of species identified by HPLC and confirm results of the literature [50].

4. Conclusions

The surface modification of titania by gold and/or nitrogen was successfully performed by using laser pyrolysis method. The as-synthesized materials show higher activity compared to TiO₂ P25 under UV illumination for degradation of model organic pollutants (formic, acetic and propionic acids). However, co-modification of laser synthesized TiO₂ with N and Au induces a decrease of the degradation rate of carboxylic acids in comparison with single modification by Au. TRMC results showed that under irradiation with UV light, the modification by Au improves photocatalytic efficiency of TiO₂ due to more efficient transfer of electrons to the surface. On the contrary, presence of N causes recombination of charges, and thus gives rise to lower photoactivity in both Au/N-TiO₂ and N-TiO₂ samples. EPR investigations confirmed the presence of two radical species in N-TiO₂ and Au/N-TiO₂ samples. That result has never been observed with N-TiO₂ synthesized by other methods, it seems to be specific to nanoparticles obtained by laser pyrolysis. As a complement, the intermediate species detected by EPR and HPLC allow proposing a reaction mechanism involved in the photo-oxidation of aliphatic organic acids. In order to improve photo-efficiency, it would be interesting to increase the size of gold nanoparticles and take advantage of surface plasmon resonance favoring activity in the visible range. In the same way, a better control of N doping favoring interstitial or substitutional doping would allow decreasing recombination of charges.

Disclosure statement

No potential conflict of interest was reported by the authors.

References

- [1] Pelaez M, Nolan NT, Pillai SC, et al. A review on the visible light active titanium dioxide photocatalysts for environmental applications. *Appl Catal B Environ.* 2012;125(1):331–349.
- [2] Lan Y, Lu Y, Ren Z. Mini review on photocatalysis of titanium dioxide nanoparticles and their solar applications. *Nano Energy.* 2013;2(5):1031–1045.
- [3] Asahi R, Morikawa T, Irie H, et al. Nitrogen-doped titanium dioxide as visible-light-sensitive photocatalyst:

- designs, developments, and prospects. *Chem Rev.* **2014**;114(19):9824–9852.
- [4] Chatterjee D, Dasgupta S. Visible light induced photocatalytic degradation of organic pollutants. *J Photochem Photobiol C Photochem Rev.* **2005**;6(2-3):186–205.
- [5] Daghbir R, Drogui P, Robert D. Modified TiO₂ for environmental photocatalytic applications: a review. *Ind Eng Chem Res.* **2013**;52:3581–3599.
- [6] Kang QM, Yuan BL, Xu JG, et al. Synthesis, characterization and photocatalytic performance of TiO₂ codoped with bismuth and nitrogen. *Catal Lett.* **2011**;141(9):1371–1377.
- [7] Liu H, Dong X, Li G, et al. Synthesis of C, Ag co-modified TiO₂ photocatalyst and its application in waste water purification. *Appl Surf Sci.* **2013**;271:276–283.
- [8] Gomathi Devi L, Kavitha R. Review on modified N-TiO₂ for green energy applications under UV/visible light: selected results and reaction mechanisms. *RSC Adv.* **2014**;4(54):28265–28299.
- [9] Mahy JG, Lambert SD, Léonard GL, et al. Towards a large scale aqueous sol-gel synthesis of doped TiO₂: study of various metallic dopings for the photocatalytic degradation of p-nitrophenol. *Journal Photochem Photobiol A Chem.* **2016**;329:189–202.
- [10] Gnanasekaran L, Hemamalini R, Saravanan R, et al. Intermediate state created by dopant ions (Mn, Co and Zr) into TiO₂ nanoparticles for degradation of dyes under visible light. *J Mol Liq.* **2016**;223:652–659.
- [11] Jafari S, Mohammadi MR, Madaah Hosseini HRM. Impact of morphology and nitrogen and carbon codoping on photocatalytic activity of TiO₂ as environmental catalysts. *Ind Eng Chem Res.* **2016**;55:12205–12212.
- [12] Zaleska A. Doped-TiO₂: a review. *Recent Patents Eng.* **2008**;2(3):157–164.
- [13] Grabowska E, Marchelek M, Klimczuk T, et al. Noble metal modified TiO₂ microspheres: Surface properties and photocatalytic activity under UV-vis and visible light. *J Mol Catal A Chem.* **2016**;423:191–206.
- [14] Méndez-Medrano MG, Kowalska E, Lehoux A, et al. Surface modification of TiO₂ with Au nanoclusters for efficient water treatment and hydrogen generation under visible light. *J Phys Chem C.* **2016**;120(43):25010–25022.
- [15] Bouhadoun S, Guillard C, Dapozze F, et al. One step synthesis of N-doped and Au-loaded TiO₂ nanoparticles by laser pyrolysis: application in photocatalysis. *Appl Catal B Environ.* **2015**;174-175:367–375.
- [16] Livraghi S, Paganini MC, Giamello E, et al. Origin of photoactivity of nitrogen-doped titanium dioxide under visible light. *J Am Chem Soc.* **2006** Dec 13;128(49):15666–15671.
- [17] Livraghi S, Votta A, Paganini MC, et al. The nature of paramagnetic species in nitrogen doped TiO₂ active in visible light photocatalysis. *Chem Commun.* **2005**;4:498–500.
- [18] Di Valentin C, Finazzi E, Pacchioni G, et al. N-doped TiO₂: theory and experiment. *Chem Phys.* **2007**;339(1-3):44–56.
- [19] Hai Z, El Kolli N, Uribe DB, et al. Modification of TiO₂ by bimetallic Au–Cu nanoparticles for wastewater treatment. *J Mater Chem A.* **2013**;1(36):10829.
- [20] Hoffmann MR, Martin ST, Choi W, et al. Environmental applications of semiconductor photocatalysis. *Am Chem Soc.* **1995**;95:69–96.
- [21] Colbeau-Justin C, Kunst M, Huguenin D. Structural influence on charge-carrier lifetimes in TiO₂ powders studied by microwave absorption. *J Mater Sci.* **2003**;38(11):2429–2437.
- [22] Tahiri Alaoui O, Herissan A, Le Quoc C, et al. Elaboration, charge-carrier lifetimes and activity of Pd-TiO₂ photocatalysts obtained by gamma radiolysis. *J Photochem Photobiol A.* **2012**;242:34–43.
- [23] Fonash SJ. *Solar cell device physics.* New York, NY: Academy Press; **1981.**
- [24] Asahi R, Morikawa T, Ohwaki T, et al. Visible-light photocatalysis in nitrogen-doped titanium oxides. *Science.* **2001**;293(5528):269–271.
- [25] Yang G, Jiang Z, Shi H, et al. Preparation of highly visible-light active N-doped TiO₂ photocatalyst. *J Mater Chem.* **2010**;20(25):5301–5309.
- [26] Duta L, Popescu C, Popescu A, et al. Nitrogen-doped and gold-loaded TiO₂ photocatalysts synthesized by sequential reactive pulsed laser deposition. *Appl Phys A.* **2014**;117(1): 97–101.
- [27] Gazsi A, Schubert G, Pusztai P, et al. Photocatalytic decomposition of formic acid and methyl formate on TiO₂ doped with N and promoted with Au. Production of H₂. *Int J Hydrogen Energy.* **2013**;38(19):7756–7766.
- [28] Amadelli R, Samiolo L, Borsa M, et al. N-TiO₂ Photocatalysts highly active under visible irradiation for NOX abatement and 2-propanol oxidation. *Catal Today.* **2013**;206(2):19–25.
- [29] Wang J, Tafen DN, Lewis JP, et al. Origin of photocatalytic activity of Nitrogen-doped TiO₂ nanobelts. *J Am Chem Soc.* **2009**;131(34):12290–12297.
- [30] Asahi R, Morikawa T. Nitrogen complex species and its chemical nature in TiO₂ for visible-light sensitized photocatalysis. *Chem Phys.* **2007**;339(1-3):57–63.
- [31] Okumura M, Coronado JM, Soria J, et al. EPR Study of CO and O₂ interaction with supported Au catalysts. *J Catal.* **2001**;203(1):168–174.
- [32] Kumar CP, Gopal NO, Wang TC. EPR investigation of TiO₂ nanoparticles with temperature-dependent properties. *J Phys Chem B.* **2006**;110:5223–5229.
- [33] Li Y, Hwang DS, Lee NH, et al. Synthesis and characterization of carbon-doped titania as an artificial solar light sensitive photocatalyst. *Chem Phys Lett.* **2005**;404(1-3):25–29.
- [34] Livraghi S, Paganini MC, Chiesa M, et al. Trapped molecular species in N-doped TiO₂. *Res Chem Intermed.* **2007**;33(8):739–747.
- [35] Livraghi S, Chierotti MR, Giamello E, et al. Nitrogen-doped titanium dioxide active in photocatalytic reactions with visible light: a multi-technique characterization of differently prepared materials. *J Phys Chem C.* **2008**;112(44):17244–17252.
- [36] Di Valentin C, Pacchioni G, Selloni A, et al. Characterization of paramagnetic species in N-Doped TiO₂ powders by EPR spectroscopy and DFT calculations. *J Phys Chem B.* **2005**;109(23):11414–11419.
- [37] Barolo G, Livraghi S, Chiesa M, et al. Mechanism of the photoactivity under visible light of N-doped titanium dioxide. charge carriers migration in irradiated N-TiO₂ investigated by electron paramagnetic resonance. *J Phys Chem C.* **2012**;116(39):20887–20894.
- [38] Konstantinova EA, Kokorin AI, Lips K, et al. EPR study of the illumination effect on properties of paramagnetic centers in nitrogen-doped TiO₂ active in visible light photocatalysis. *Appl Magn Reson.* **2009**;35(3):421–427.

- [39] Howe RF, Gratzel M. EPR observation of trapped electron in colloidal TiO_2 . *J Phys Chem.* **1985**;89(21):4495–4499.
- [40] Meichtry JM, Colbeau-Justin C, Custo G, et al. TiO_2 -photocatalytic transformation of Cr (VI) in the presence of EDTA : comparison of different commercial photocatalysts and studies by time resolved microwave conductivity. *Appl Catal B Environ.* **2014**;144:189–195.
- [41] Boujday S, Wünsch F, Portes P, et al. Photocatalytic and electronic properties of TiO_2 powders elaborated by sol-gel route and supercritical drying. *Sol Energy Mater Sol Cells.* **2004**;83(4):421–433.
- [42] Emilio CA, Litter MI, Kunst M, et al. Phenol photodegradation on platinized- TiO_2 photocatalysts related to charge-carrier dynamics. *Langmuir.* **2006**;22(8):3606–3613.
- [43] Kumar SG, Devi LG. Review on modified TiO_2 photocatalysis under UV/visible light: selected results and related mechanisms on interfacial charge carrier transfer dynamics. *J Phys Chem A.* **2011**;115(46):13211–13241.
- [44] Serpone N, Martin J, Horikoshi S, et al. Photocatalyzed oxidation and mineralization of C1–C5 linear aliphatic acids in UV-irradiated aqueous titania dispersions—kinetics, identification of intermediates and quantum yields. *J Photochem Photobiol A Chem.* **2005**;169(3):235–251.
- [45] Buxton GV, Greenstock CL, Helman WP, et al. Critical-review of rate constants for reactions of hydrated electrons, hydrogen-atoms and hydroxyl radicals ($\cdot\text{OH}/\cdot\text{O}\cdot$) in aqueous-solution. *J Phys Chem.* **1988**;17: 513–886.
- [46] Kaise M, Nagai H, Tokuhashi K, et al. Electron spin resonance studies of photocatalytic interface reactions of suspended M/TiO_2 ($\text{M} = \text{Pt}, \text{Pd}, \text{Ir}, \text{Rh}, \text{Os},$ or Ru) with alcohol and acetic acid in aqueous media. *Langmuir.* **1994**;10(5):1345–1347.
- [47] Nosaka Y, Koenuma K, Ushida K, et al. Reaction mechanism of the decomposition of acetic acid on illuminated TiO_2 powder studied by means of in situ electron spin resonance measurements. *Langmuir.* **1996**;12:736–738.
- [48] Gandhi V, Mishra M, Joshi PA. Titanium dioxide catalyzed photocatalytic degradation of carboxylic acids from waste water: a review. *Mater Sci Forum.* **2012**;712:175–189.
- [49] Shkrob IA, Chemerisov SD. Light induced fragmentation of polyfunctional carboxylated compounds on hydrated metal oxide particles: from simple organic acids to peptides. *J Phys Chem C.* **2009**;113(39):17138–17150.
- [50] Sakata T, Kawai T, Hashimoto K. Heterogeneous photocatalytic reactions of organic acids and water. New reaction paths besides the photo-Kolbe reaction. *J Phys Chem.* **1984**;88(11):2344–2350.